TESCAN

A unique combination of Plasma FIB and field-free UHR SEM for the widest range of multiscale materials characterization applications

1 mm cross-section through a Li-ion battery electrode

TESCAN AMBER X

- ✓ High throughput, large area FIB milling up to 1 mm
- ✓ Ga-free microsample preparation
- ✓ Ultra-high resolution, field-free FE-SEM imaging and analysis
- ✓ In-column SE and BSE detection
- ✓ Spot optimization for high-throughput, multi-modal FIB-SEM tomography
- ✓ Superior field of view for easy navigation
- ✓ Essence™ easy-to-use, modular graphical user interface

For more information visit

www.tescan.com

ADVANCED ENERGY MATERIALS
www.advenergymat.de

Transparent, High-Charge Capacity Metal Mesh Electrode for Reversible Metal Electrodeposition Dynamic Windows with Dark-State Transmission <0.1%

*Andrew L. Yeang, Tyler S. Hernandez, Michael T. Strand, Daniel J. Slotcavage, Eldho Abraham, Ivan I. Smalyukh, Christopher J. Barile, and Michael D. McGehee**

Dynamic windows allow user control over light and heat flow to save energy and maximize comfort. Reversible metal electrodeposition (RME) dynamic windows can uniquely tint to a color-neutral privacy state (0.1% visible light transmission). The design parameters of transparent metal mesh counter electrodes for high-contrast RME dynamic windows: high transparency, charge capacity and surface area with low haze, sheet resistance and cost are discussed, concluding that woven metal meshes meet these design parameters. Electroplated current is measured on an indium tin oxide electrode and two meshes with different wire spacings, showing the meshes' cylindrical geometry enable them to draw more current per square area. The mesh material composition is analyzed to ensure cycling durability in a Cu—Bi electrolyte by developing a transparent mesh with an inert core (stainless steel, SS), a thin Au coating, and a high charge-capacity (1.5 C cm^{-2}) Cu—Bi outer coating. The study demonstrates that the films maintain a consistent Cu:Bi ratio and optical properties after 250 privacy cycles or 1500 cycles to 10% transmission, showing that the Cu and Bi coating is effective in keeping the films from becoming Cu rich with cycling. Finally, a 100 cm^2 device with excellent uniformity and color neutrality is demonstrated.

1. Introduction

Dynamic windows allow users to control light and heat flow into and out of buildings without obstructing their view, enabling energy savings up to 20% compared to static low-emissivity coatings due to reductions in lighting, heating, and cooling loads.[1–3] A recent study by View Inc. and Cornell University showed that dynamic window implementation greatly reduces eye strain, headaches, and drowsiness, resulting in a 2% increase in worker productivity.[4] Despite these advantages, dynamic windows, which traditionally operate using electrochromic metal oxides[5,6] or conductive organic molecules[7–9] have failed to significantly penetrate the market due to issues related to color, cost, scale, and optical dynamic range.[5,8] View, Sage, and Halio are the current leaders in the dynamic window market. They have made dynamic windows aimed for commercial settings due to their current optical contrast limits.[10–12] Most of their products have a maximum transmission between 58% and 64%[10–12] and reach a "glare control" transmission state, which is defined as 1% visible light transmission (VLT), to reduce occupant discomfort and eye strain.[13] Reaching the residential market, however, requires achieving darker states for privacy and sleeping along with a higher degree of color neutrality.[14] Halio has recently developed a product that enables their windows to reach a "privacy state," which they internally define as 0.1% VLT.[12] This device construction comes

A. L. Yeang, T. S. Hernandez, M. T. Strand, M. D. McGehee
Department of Chemical and Biological Engineering
University of Colorado Boulder
Boulder, CO 80303, USA
E-mail: michael.mcgehee@colorado.edu

T. S. Hernandez
Department of Chemistry
Stanford University
Stanford, CA 94305, USA

M. T. Strand, D. J. Slotcavage
Department of Materials Science and Engineering
Stanford University
Stanford, CA 94305, USA

E. Abraham, I. I. Smalyukh
Department of Physics
University of Colorado Boulder
Boulder, CO 80309, USA

E. Abraham, I. I. Smalyukh, M. D. McGehee
Renewable and Sustainable Energy Institute: National Renewable Energy Laboratory and University of Colorado at Boulder
Boulder, CO 80303, USA

I. I. Smalyukh, M. D. McGehee
Materials Science and Engineering Program
University of Colorado Boulder
Boulder, CO 80303, USA

C. J. Barile
Department of Chemistry
University of Nevada Reno
Reno, NV 89503, USA

M. D. McGehee
National Renewable Energy Laboratory
Golden, CO 80401, USA

The ORCID identification number(s) for the author(s) of this article can be found under https://doi.org/10.1002/aenm.202200854.

DOI: 10.1002/aenm.202200854

from stacking two of their dynamic glazings together, which increases cost and reduces their clear state transmission from 64% to 50%.[12]

Dynamic windows based on reversible metal electrodeposition (RME) are an exciting alternative approach and have the potential to overcome the issues associated with traditional dynamic windows.[14–19] RME dynamic windows modulate light by the reversible electrodeposition of metal on and off a transparent conducting oxide (TCO) decorated with Pt nanoparticles. These windows typically use an aqueous electrolyte containing metal cations (e.g., Cu^{2+} and Bi^{3+}). Applying a cathodic potential on the TCO reduces the metal cations to a color-neutral metallic film across the TCO surface to block light, tinting the window. A reverse in polarity oxidizes the metal back into solution in a process called "bleaching," returning the window to its transparent state, which is 60–85%, depending on device architecture.[14,16–19] Thus far for RME dynamic windows, significant attention has been given to the working electrode TCO and the electrolyte.[14,16–19] Pt nanoparticles have been anchored to the TCO surface to improve metal nucleation and RME without significantly affecting electrode transmissivity or conductivity.[16,18] A Cu—Bi electrolyte has also been developed that demonstrates color-neutral tinting and impressive durability.[17,19] More recently, we have shown that a small amount (0.1 w/v%) of a polymer (poly-vinyl alcohol) added to the electrolyte prevents dendrite growth and enables RME dynamic windows to reach a privacy tinted state due to a smooth and compact electrodeposited film.[14] Because RME dynamic windows achieve this privacy state using one dynamically tinting layer and use solution processed techniques, they have the potential to be much cheaper and open up the residential market.

To reach a privacy state, current RME dynamic windows shuttle ≈150 mC cm^{-2} between the working and counter electrode.[14] A robust counter electrode must have enough capacity to charge balance the working electrode reaction while maintaining desired window properties (high transparency and low haze). Some RME systems use redox shuttles in the electrolyte[15,20,21] (e.g., 3 $Br^- \leftrightarrows Br_3^-$, **Figure 1**a) or ion intercalation materials as the counter electrode material[22–25] (e.g., NiO_x and various hexacyanoferrates, Figure 1b) for the counter reactions. Redox shuttles are not ideal for RME as the 3 $Br^- \leftrightarrows Br_3^-$ reaction is colored.[19] Ion intercalation materials (e.g., Li^+ intercalation into NiO_x) help by enabling dual tinting electrodes, but these electrodes are typically slightly colored in the clear state.[26–29] To reach higher capacities, the ion intercalation materials need to be thicker, decreasing their transparency due to Beer's law. Metal meshes can be optimized as transparent electrodes because of their high transmissivity and low resistivity[30–32] and offer an attractive approach to designing a high charge-capacity electrode.[14,18,19,33] Metal meshes also simplify window design by having the same materials reversibly electroplated on both electrodes as shown in Figure 1c. We have previously described dynamic windows made with Cu metal mesh electrodes bought off the shelf.[14,18,19]

In this work, we outline the design considerations for a metal mesh counter electrode, focusing on the mesh geometry and material composition. First, we outline the benefits of using metal meshes as transparent, low-haze, low-sheet resistance, and high charge-capacity electrodes. We choose woven metal meshes for the counter electrode due to their low cost and high electrochemically active surface area. An additional benefit to using metal meshes is that their cylindrical geometry enables more current to be drawn despite the less electrochemically active area per square compared to the planar TCO, which enables control over bleaching speed while maintaining high transmission. Our experiments show that Cu mesh counter electrodes increase the Cu^{2+} concentration of the Cu—Bi electrolyte over privacy cycling, resulting in optical and electrochemical degradation. We develop a woven mesh incorporating a stainless-steel (SS) core that is electrochemically inert. To improve plating of Cu and Bi on SS, which is difficult due to native oxides on the SS surface, we electroplate an Au-capping layer that improves Cu—Bi adhesion. This mesh design (Cu—Bi Au-SS mesh) has a high charge capacity (1.5 C cm^{-2} without significantly affecting the electrode transparency (<2% decrease) or haze (<1% decrease) and shows an improvement in durability. We demonstrate 250 privacy cycles and 1500 cycles to 10% transmission without significantly changing the

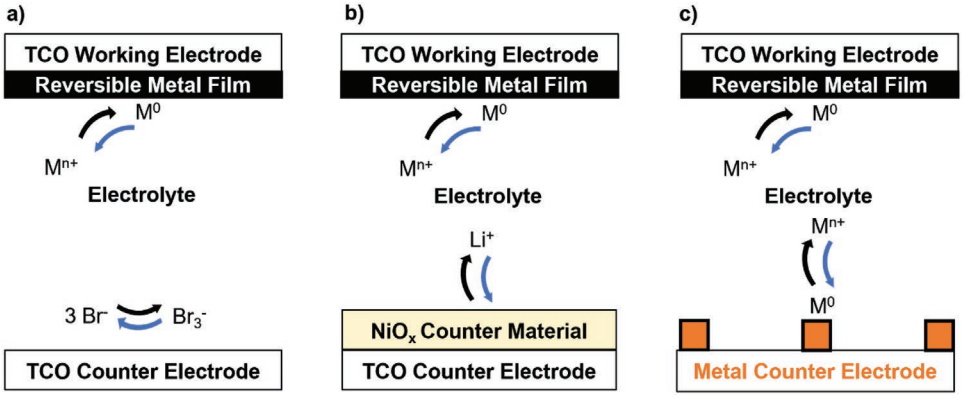

Figure 1. Schematic showing examples of different counter electrode options for RME dynamic windows: a) redox shuttles where many electrolytes use Br^- as a counter ion to the metal salts, b) ion intercalation materials where Li^+ is already in the electrolyte to improve ionic conductivity, or c) metal counter electrodes where the same metals from the reversible metal film are reversibly plated onto the metal counter electrode. Black arrows indicate reactions for window tinting and blue arrows indicate reactions for window bleaching. All architectures show use RME ($M^{n+} \leftrightarrows M^0$) on a TCO working electrode to deposit a metal film to modulate light.

Table 1. Properties of Cu and SS woven mesh from TWP, Inc. See Figure S4, Supporting Information, for transmission properties and Note S2, Supporting Information, for electrochemical properties.

Property	Cu mesh	Stainless steel (SS) mesh
Wire diameter [μm]	30.48	30.48
Wire pitch [μm]	224	476
Transparency, no substrate [%]	75.6	87.3
Sheet resistance [Ω □$^{-1}$]	0.045	2.05
FoM	27 906	1309
Haze, with glass substrate [%]	4.6	1.7
Off-the-shelf RME capacity (C cm^{-2} window)	15.64	0
Electrochemically active area per square area [%]	75	37

electrolyte composition. We discuss how the opacity of the dark state in cycling affects the cycle life of an RME dynamic window, showing that shuttling less metal improves cycle life. Finally, we fabricate a 10 cm × 10 cm device using this Cu—Bi Au-SS mesh.

2. Results and Discussion

2.1. Geometric Considerations: Optimizing Metal Meshes for Transparency and Electrochemically Active Area

Metal mesh electrodes are a leading candidate for transparent conductors with the ability to optimize for transparency and sheet resistance by varying the line width and line pitch.[34] An increase in line width or reduction in line pitch will decrease sheet resistance with the tradeoff of decreased transparency.

Metal mesh counter electrodes are plane-parallel with the TCO, making the ion diffusion distance nearly uniform from the counter electrode to the working electrode and allowing uniform plating across the working electrode (Figure S1, Supporting Information). The Cu free-standing woven mesh is bought off the shelf from TWP Inc. with a wire diameter of 30.48 μm and a pitch of 244 μm. pitch. The measured transparency of the Cu metal mesh is 75.6%, and the measured sheet resistance is 0.045 Ω □$^{-1}$, giving it a high transparent conductor figure of merit of 27 906 as defined by Dressel and Grüner (Equation (1)):

$$\Phi_{TE} = \frac{\sigma_{dc}}{\sigma_{opt}} = \frac{188.5}{R_{sh}\left(\frac{1}{T_{550\,nm}^{1/2}} - 1\right)} \quad (1)$$

This figure of merit relates the relationship between direct current conductivity, σ_{dc}, and optical conductivity at 550 nm, σ_{opt}.[35] Stainless steel (SS) will be explored later in the study, and its analogous mesh properties are shown in **Table 1**. Both of these woven meshes exhibit exceptional figures of merit as transparent conductors, far exceeding the typical industrial standard of at least 350.[36–38] For RME dynamic windows, low sheet resistance transparent conductors reduce the voltage drop from edge to center of a large scale window (Equation S1, Supporting Information)[18] We show in Note S1, Supporting Information, that the sheet resistance of indium tin oxide (ITO) (≈7–10 Ω □$^{-1}$) limits the size of an RME dynamic window with uniform tinting (Figure S2, Supporting Information). Haze is defined as the amount of diffuse transmitted light divided by total transmitted light. Less than 3% haze is typically the threshold where a clear view is necessary.[34,39] The haze values (4.6% for Cu mesh and 1.7% for SS mesh) are primarily related to the geometry of the mesh. The bigger spacing between the wires in the SS mesh significantly reduces the diffuse transmission and the haze to acceptable levels.

Next, we explore how metal lines of different widths are perceived using photolithography to make meshes with lines that are thinner than can be obtained in woven meshes. After patterning ITO using photolithography and electroplating Cu to different line widths from 5 to 50 μm, we show that 10-μm lines are effectively invisible to the human eye (Figure S3, Supporting Information), consistent with previous literature,[40] while 25-μm lines are barely visible.

Electrochemical capacity to balance the working electrode reaction is equally important. If all of the Cu from the mesh were transferred to the working electrode, the capacity would be 15.64 C cm^{-2}, which is ≈100× the capacity needed to switch the RME dynamic window to privacy (Table 1, see Note S2, Supporting Information, for detailed calculation).

For RME dynamic windows, it is ideal to have the highest transparency without compromising switching speed. We show that varying the metal counter electrode area relative to the working electrode (Pt-modified ITO, "Pt-ITO") area does not significantly affect the window tinting speed but has a significant impact on window bleaching speed (Figure S5, Supporting Information). The reason for this difference is due to the diffusion to the electrode surfaces. For tinting, the metal ions diffuse from the bulk to the surface of the Pt-ITO active area. Metal oxidation from the metal counter electrode is not limiting as metal can readily be oxidized from this electrode (Figure S6a,b, Supporting Information). Upon bleaching, however, the diffusion of the metal ions is constrained to the active area of the metal electrode, which has a different area (Figure S6c,d, Supporting Information). Again, the metal oxidation from the metal-plated Pt-ITO electrode is not limiting, until all the metal is oxidized, and the window returns to transparent. For a more detailed explanation, see Note S3, Supporting Information. We also discuss the RME tinting speed compared to other electrochromic technologies in Note S4, Supporting Information, and conclude that we have a wider dynamic range and a comparable switching time.[41]

While 10-μm lines are desired, processing these meshes at scale can increase cost significantly. Printing and other solution processes have been used to make large-scale metal mesh electrodes with high figures of merit.[34,36,40,42,43] A woven metal mesh (Cu or SS) with 30-μm diameter, however, is commercially available (TWP, Inc.). Perhaps the biggest advantage to using a free-standing woven mesh compared to other fabrication techniques such as embedding a metal mesh[36,42] and photolithography[43] is that a free-standing woven mesh maximizes the active area for electrochemical

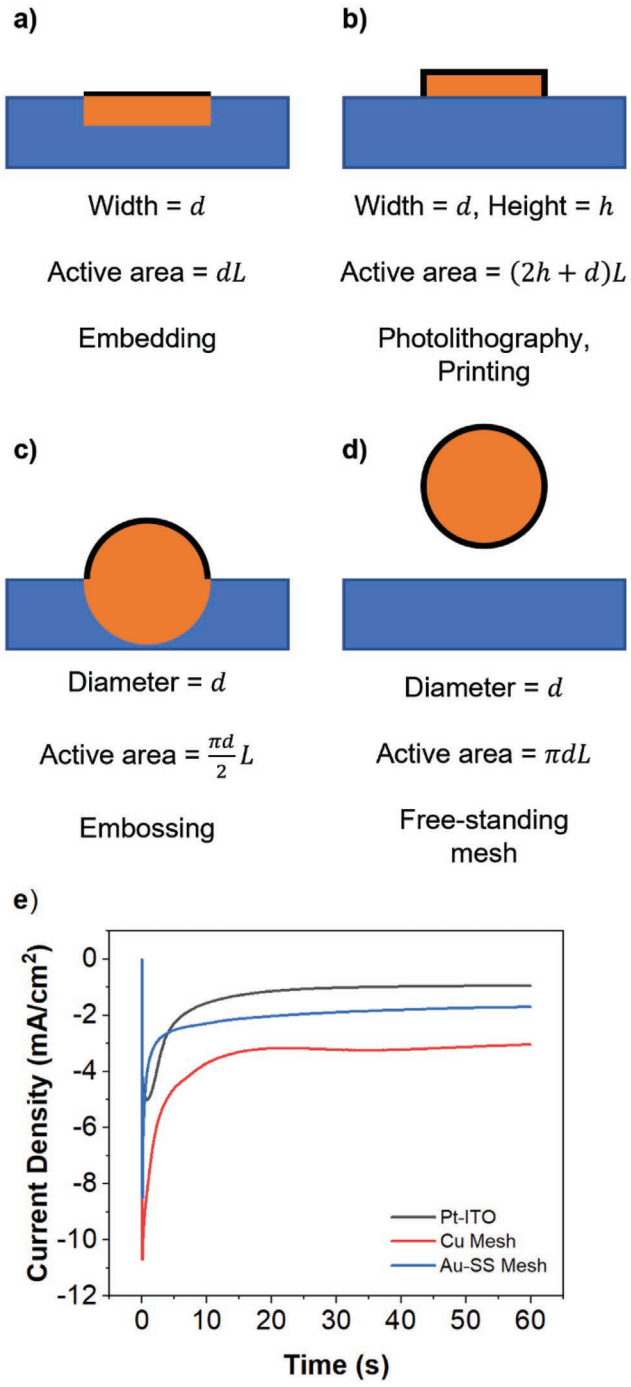

Figure 2. a–d) Various metal mesh geometries and their electrochemically active areas shown in black for given projected area. Fabrication examples listed underneath. Metal electrode shown in orange and non-conductive backing (e.g., glass or plastic) shown in blue. *L* is the length of the electrode. e) Current density per square area versus time for (black) Pt-ITO, (red) Cu mesh, and (blue) Au coated SS mesh for metal deposition induced at –0.7 V versus Ag/AgCl for 1 min using the Cu—Bi electrolyte.

reactions without significantly affecting the window's clear state transparency (**Figure 2**a–d). Figure 2e shows the current density per square area versus time for half cells plating Cu and Bi onto a Pt-ITO (planar surface), a Cu mesh (cylindrical wires), and an Au coated SS mesh (cylindrical wires). Despite the active areas being 75% and 37% of the total square area of the Pt-ITO electrode for the Cu mesh and Au-SS mesh, respectively (Table 1), they draw more current than the planar Pt-ITO electrode due to their cylindrical geometry (See Note S5, Supporting Information, for a detailed discussion).[44–46] Thus, the free-standing woven mesh has the fastest window bleaching speed for a given electrode geometry, and the design of the mesh can limit the rate at which the window bleaches. Despite half of the mesh facing the glass backing, the front and back sides of a free-standing Cu mesh show nearly the same ratio of Cu:Bi after 10 privacy cycles using energy-dispersive X-ray spectroscopy (EDS), confirming the entire immersed surface area is electrochemically active (Figure S11, Supporting Information). For a discussion on an ideal mesh design using different wire diameters, see Note S6, Supporting Information,.

2.2. Materials Consideration: Cu and Stainless-Steel Metal Meshes for Privacy Cycling RME Devices

Having established the geometric design considerations for a metal mesh counter electrode for RME dynamic windows, we now investigate potential materials used for the metal mesh counter electrode. **Table 2** shows various materials that could be used for a counter electrode mesh material and relevant material properties including conductivity, redox properties, raw material cost, and commercial availability as a mesh. All these materials are highly conductive and thus would have low sheet resistances. The standard reduction potentials theoretically should be more positive than those of the metals deposited such that the mesh material should remain inert. Due to standard reduction potential, material cost and/or the availability to purchase as a woven mesh, the most promising options in our acidic Cu—Bi electrolyte are Cu and stainless steel (SS), which will be the focus of the study.

2.2.1. Studies with Cu Metal Mesh Electrodes

Cu has been used as a counter electrode in our most recent RME dynamic window designs because it is a low-cost material with one of the highest conductivities.[14,18,19] We found that a two-electrode RME dynamic window using a Cu mesh counter electrode achieves color-neutral tinting to privacy on cycle 1 by tinting the window at –0.7 V, which takes 276 s to pass the necessary 159 mC cm^{-2}. The Cu mesh device maintains a color neutral privacy transmission state over 250 cycles (**Figure 3**a). The corresponding reflection data (Figure 3b), however, shows a peak in reflection starting at 550 nm by cycle 200, which becomes more pronounced by cycle 250.

The coloration efficiency decays as a function of cycle number, dropping from 18.3 cm^2 C^{-1} on cycle 1 to 13.9 cm^2 C^{-1} by cycle 250 (Figure 3c). Coloration efficiency is defined as the change in transmission state divided by the charge passed for a given window area to achieve that transmission state and is a metric to determine how efficient a device blocks light. This drop in coloration efficiency also means that charge passed

Table 2. Various mesh materials and relevant properties as a counter electrode material for RME dynamic windows. Costs are for bulk metals and were found on October 11, 2021 using https://price.metal.com/.

Mesh material	Conductivity [S m^{-1}]	Standard reduction potential (V versus SHE)	Raw metal cost ($/kg)	Availability as a mesh
Cu	5.96×10^7	0.337	11	Commercially available (TWP, Unique Wire, etc.)
Stainless Steel	1.45×10^6	N/A	4.6	Commercially available (TWP, Unique Wire, etc.)
Ni	1.43×10^7	−0.25	22.6	Commercially available (Unique Wire)
Zn	1.69×10^7	−0.7618	3.6	Not commercially available
Bi	7.75×10^5	0.308	7.7	Not commercially available
Pb	4.55×10^6	−0.126	2.3	Toxic—not commercially available
Ag	6.30×10^7	0.7996	732	Not commercially available
Au	4.10×10^7	1.83	58088	Not commercially available

cannot be used as a proxy for window transmission state, necessitating another mechanism for the user to know the transmission state of the window, such as a photodetector. The growing peak in reflection and drop in coloration efficiency over cycling suggest an increase in [Cu^{2+}] and that more Cu is plated[16,47] from the electrolyte after many cycles. To confirm this hypothesis, we conducted EDS on the metal deposits from the cycled electrolyte and compared the results to those from fresh electrolyte. Initially, the ratio of Cu:Bi in the metal film is 3.2 (Figure S13, Supporting Information). After 250 privacy cycles in a Cu mesh device, this ratio rises significantly to 13.8 (Figure S14, Supporting Information). This increase in the Cu:Bi ratio of the metal film after extensive privacy cycling confirms that [Cu^{2+}] is increasing into the electrolyte, thus inducing a change in the overall composition of the metal film. For a detailed discussion about the implications of using a Cu mesh on the electrolyte on the first cycle, see Note S7, Supporting Information.

2.2.2. Improvements to the Metal Mesh Counter Electrode Using an Inert Core (Stainless-Steel) and Shell (Electroplated Au)

The Cu mesh has the propensity to increase [Cu^{2+}] into the electrolyte over cycling because it is an electrochemically active material (Table S1, Supporting Information). In **Figure 4**a, we show a cyclic voltammogram (CV) in an electrolyte without active metals (no Cu or Bi, "blank" electrolyte). The rise in oxidative current beyond 0.1 V using the Cu mesh (black curve) indicates Cu metal oxidation. Stainless steel (SS) is chemically inert and possesses a high conductivity (1.45×10^6 S m^{-1} and measured sheet resistance of 2.05 Ω $\square^{-1}$), making it an excellent candidate as a counter electrode material, as it has been used in other Zn-based systems.[33,48] A CV of the SS mesh in the blank electrolyte shows no Faradaic current in the same potential range, indicating that there are no electrochemical side reactions in the voltage range for RME dynamic windows (Figure 4a, red curve, Table 1). The woven SS mesh was purchased with the same wire diameter as the Cu mesh (30.48 µm), but with a higher pitch (476 µm), which increases the transmission of the mesh by ≈10% (Table 1).

Because SS is electrochemically inactive in this potential range, bare SS has no capacity to balance charge in an RME dynamic window (Figure 4a, red curve and Table 1). Pre-depositing Cu and Bi via electrodeposition gives the SS electrode capacity to balance Cu and Bi electrodeposition on the working electrode. Additionally, it provides a symmetric electrochemical system where RME of Cu and Bi can occur on both the working and counter electrodes, thus eliminating degradative side reactions and reducing complexity.

Native oxides on the SS surface contribute to the chemical robustness of SS but also make it difficult to electroplate metals onto bare SS.[49] We electrocleaned the mesh using a process described in more detail in the Experimental Section. A thin layer of electroplated metal, known as a "strike," is often used to improve metal electroplating and subsequent adhesion on SS surfaces. The most common of these strikes is Ni.[49] A Ni strike was explored in this study but was ultimately not used due to its oxidation by soaking in our electrolyte after 1 week (see Note S8, Supporting Information); we thus opted for a more noble metal in Au. The aqueous TriVal Gold strike bath contains potassium auricyanide and hydrochloric acid (Gold Plating Services). The Au strike on SS mesh fully covers the SS mesh surface with ≈0.2 µm increase in total wire thickness (Figure S18, Supporting Information), while remaining electrochemically inert in the desired potential range (Figure 4a, blue curve). For RME dynamic windows, the Au-SS mesh also shows improvement compared to the bare SS mesh in metal nucleation by decreasing the onset potential for Cu−Bi deposition by 128 mV and the onset potential for Cu−Bi stripping by 84 mV (Figure 4b).

The electrodeposited metal adhesion issue on bare SS is shown by the SEM-EDS in **Figure 5**. Figure 5a shows SEM of Cu and Bi electrodeposited onto a bare SS mesh substrate. Clearly, there is a section on the bare SS mesh that is not coated, and EDS in Figure 5b confirms the uncoated section is rich in Fe, which is the largest component of SS. In contrast, Figure 5c shows SEM of Cu and Bi electrodeposited onto Au-SS mesh with full coverage (Figure 5d).

2.2.3. Implementation of the Cu−Bi Au-SS Mesh for RME Dynamic Window for Privacy Cycling

One significant advantage to using a metal mesh as a counter electrode material is the ability to simultaneously achieve

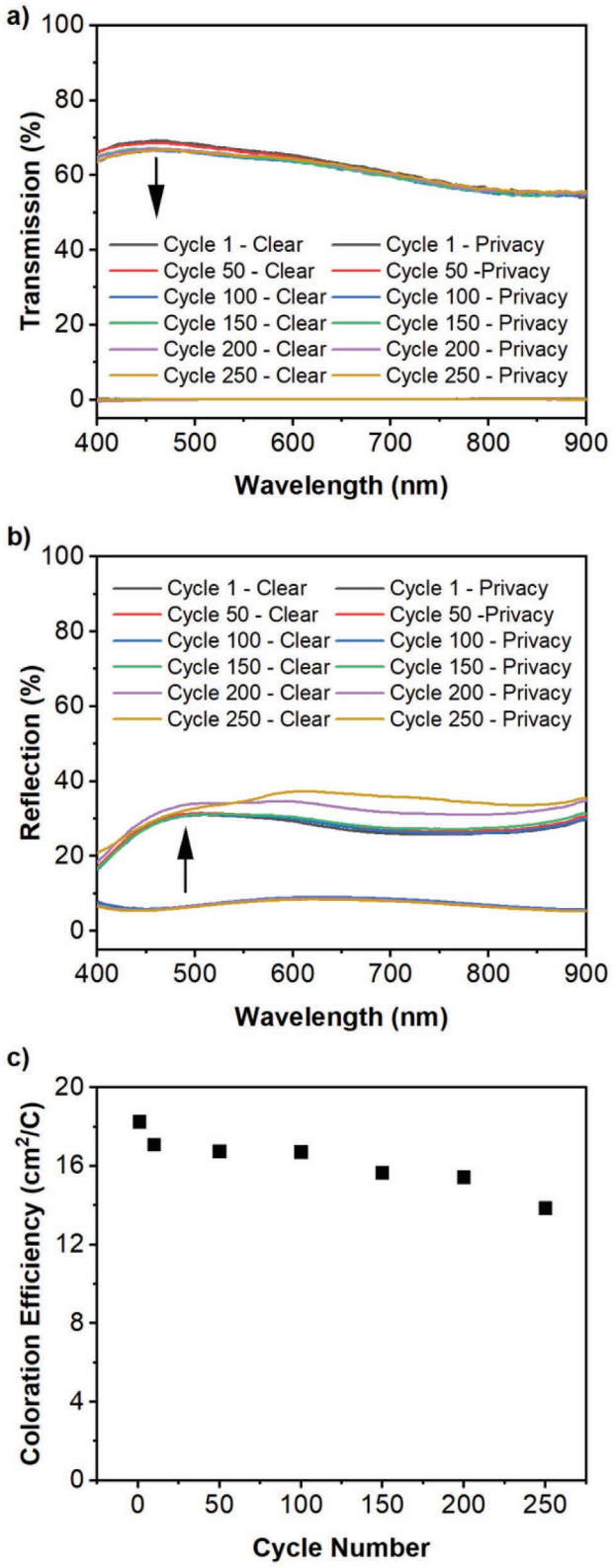

Figure 3. Cu mesh RME dynamic window device performance over 250 privacy cycles: a) transmission versus wavelength, b) reflection versus wavelength, and c) coloration efficiency as a function of cycle number. Arrows in (a) and (b) indicate direction of window tinting. Windows were tinted at −0.7 V and bleached at +0.7 V.

high transparency, low haze, and high capacity. **Table 3** shows the effects of the Au strike and pre-loading the Au strike SS mesh (Au-SS) via electrodeposition with Cu and Bi on the transmission and haze. Remarkably, plating up to 10× the capacity needed to achieve privacy state transmission on the ITO electrode does not significantly decrease the transmission (≈2% drop with an increase in total wire diameter to ≈35 µm, ≈2.5 µm additional thickness in radius on top of the Au strike) and decreases haze (from 1.7% to 0.8%), which is likely due to absorption of light from the black Cu−Bi wire coating. Thus, the Au-SS mesh electrode can be pre-loaded with and can serve as a sink of Cu and Bi metal to be reversibly electroplated without significantly affecting the clear state optics of the window. Plating just enough Cu−Bi to theoretically achieve privacy transmission (150 mC cm^{-2}) is not sufficient because not all the plated metal can be oxidized, and the device fails to reach the privacy state on cycle 1 (Figure S19, Supporting Information). Therefore, it is necessary to plate more metal to achieve the privacy state reliably. An additional benefit of the rough Cu−Bi wire coating is that the metal electrode appears black from the initial cycle, while the Cu mesh appears red-orange until after the first cycle, when Bi and Cu are plated onto the Cu mesh (Figure S20, Supporting Information).

Next, we implement this custom Au-SS metal mesh counter electrode pre-coated with Cu and Bi via electrodeposition with 10× privacy capacity into a RME dynamic window for privacy cycling (the Cu−Bi Au-SS mesh device). The clear state transmission is >70% at 550 nm, which is higher than that in commercially available electrochromic windows, where the clear state transmissions are between 58% and 64%.[10–12] The Cu−Bi Au-SS mesh device is also tinted at −0.7 V and takes 224 s to pass the required 147 mC cm^{-2}. This device maintains a color neutral privacy state over 250 cycles (**Figure 6**a). In contrast to the Cu mesh device, which had a growing peak in reflection starting at 550 nm and a continuous drop in coloration efficiency over cycling, the Cu−Bi Au-SS mesh device maintains a consistent reflection profile over cycling (Figure 6b) and sustains a consistent coloration efficiency (≈17.4 cm^2 C^{-1}) after an initial drop (from 20.3 to 17.4 cm^2 C^{-1}) in the first 10 cycles (Figure 6c). We attribute this initial drop in coloration efficiency to electrochemical conditioning, which is typical of RME systems.[50] The fact that the window has a consistent coloration efficiency (Figure S22, Supporting Information) simplifies the window design to an algorithm that can determine the transmission state of the window based on the amount of charge passed, which reduces the cost for dynamic windows. When EDS is conducted on the metal deposits after 250 cycles, the ratio of Cu:Bi is 4.8 (Figure S23, Supporting Information), which is much closer to the original ratio, which was 3.2, compared to the deposits from the Cu mesh device, which was 13.8. Thus, the metal choice on the counter electrode also plays a vital role in device durability.

2.3. Context for Cycling Conditions: Deeper Cycles Decrease Cycle Life

It is known in the battery literature that depth of discharge affects the cycle life and degradation for both Li metal[51] and

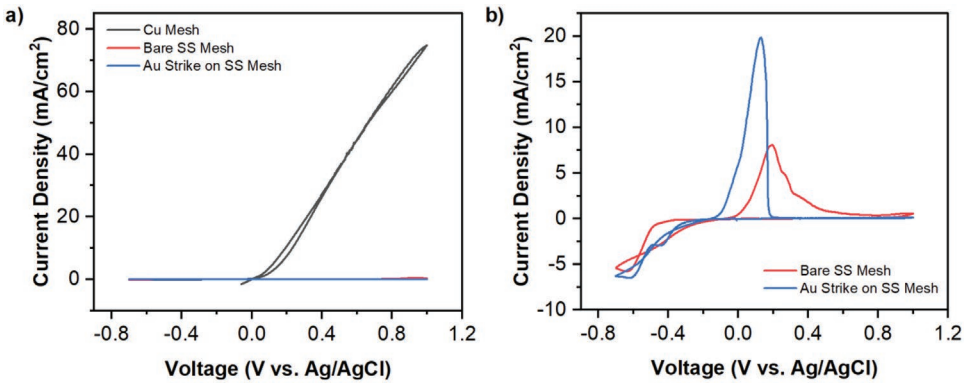

Figure 4. Cyclic voltammograms using various meshes in a) "blank" and b) full Cu—Bi electrolytes. Blank electrolyte consists of 1 M $LiClO_4$, 10 mM $HClO_4$, and 0.1 w/v% PVA. Cu—Bi electrolyte consists of the blank electrolyte plus 10 mM $Cu(ClO_4)_2$ and 10 mM $BiOClO_4$.

Li-ion batteries,[52] where a deeper depth of discharge decreases cycle life. In fact, the commonly used concept of "C rate" in batteries is based on defining the charge and discharge rates in relation to their depth of discharge. A deeper depth of discharge for batteries is analogous to cycling dynamic windows to a darker transmission state. In this work, we have focused our attention on privacy cycling where the Cu mesh device shows degradation by cycle 200. To put the 250 privacy cycles for the Cu—Bi Au-SS mesh device in context, we also cycled a device with this architecture to 10% transmission and show 1500 cycles without significant degradation in optical contrast (**Figure 7**). These differences in cycle numbers reported are consistent with what one would expect given what is known in battery literature due to the differences in cycling conditions. In both cycling conditions, dendrites form on the Cu—Bi Au-SS mesh, limiting the device cycle life (Figure S24, Supporting Information). In future work, we will explore alternate cycling conditions to avoid the dendrite growth.

2.4. Implementation into a 10 cm × 10 cm Device

Finally, we incorporate this Cu—Bi Au-SS mesh into a 10 cm × 10 cm RME device that tints uniformly and reaches the privacy state in 315 s and returns to the clear state in 115 s (**Figure 8**). The 10 cm × 10 cm window tints and bleaches slower than the 5 cm × 5 cm devices since we used a thicker electrolyte layer to avoid potential short circuiting using a free-standing woven

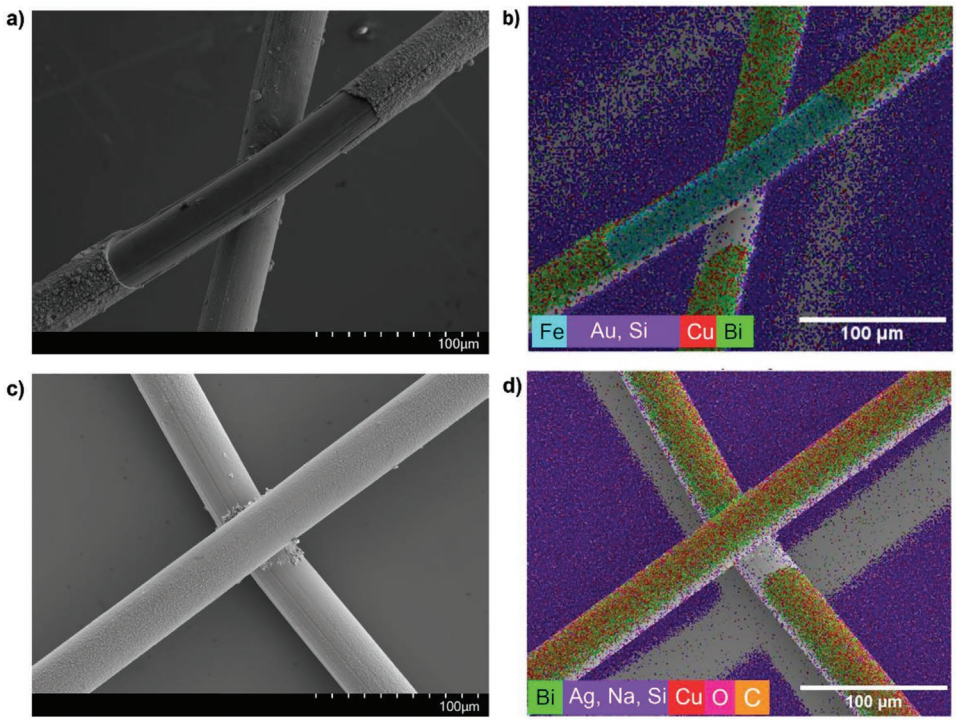

Figure 5. a) SEM and corresponding b) EDS map of 10× privacy capacity Cu—Bi plated onto the bare SS mesh. c) SEM and corresponding d) EDS of 10× privacy capacity Cu—Bi plated onto the Au-SS mesh.

Table 3. Optical properties of SS mesh preloaded with Cu and Bi for various RME window minimum tint states. Charge capacity was electrodeposited from using the Cu—Bi electrolyte. Transmission and haze measurements were completed with the metal mesh adhered to a glass substrate. Full spectra for full and diffuse transmission are shown in Figure S21, Supporting Information.

Substrate	Theoretical minimum transmission state of window	Charge capacity [mC cm^{-2}]	Transmission [%]	Haze [%]
Stainless steel mesh	N/A	0	80.5	1.7
Au strike on SS mesh	N/A	0	80.2	1.6
10% VLT	10%	50	80.2	1.0
Glare control	1%	100	80.0	0.9
Privacy	0.1%	150	79.6	1.0
10× Privacy	<<0.1%	1500	78.8	0.8

mesh over the large device. A gel electrolyte can be implemented to enable thin devices to minimize the diffusion distance between the two electrodes, allowing for faster switching speeds without the potential for a short-circuited device. For a discussion on the size of an RME window, see Note S1, Supporting Information, where we show that the limiting factor currently is the sheet resistance of the Pt-ITO electrode, not the metal mesh. Color neutrality is desired in dynamic windows as not to obstruct or taint the view. We show in Table S2, Supporting Information, that the Cu—Bi Au-SS mesh device is color neutral across a range of tint states (see Note S9, Supporting Information, for a detailed explanation).

3. Conclusions

In this work, we explore metal meshes as a counter electrode material for RME dynamic windows. We show that metal meshes simultaneously have high transparency (>75%), low haze (<5%), and low sheet resistance (<3 Ω □$^{-1}$). Metal meshes also satisfy the added electrochemical constraint of having high charge capacity, making them an excellent candidate for RME dynamic windows achieving privacy state transmission (0.1% VLT). We conclude that free-standing woven meshes offer a unique advantage over other processing techniques due to the higher exposed surface area at low cost. The cylindrical geometry of the mesh also can support more current per square area of window compared to the planar ITO surface, allowing the mesh to be designed with even higher transparency for a given bleaching speed. The use of the Cu mesh counter electrode slowly increases [Cu^{2+}] in the electrolyte over the course of 250 privacy cycles, which results in significant changes in reflection and drop in coloration efficiency. The Cu:Bi deposited onto Pt-ITO increased drastically from 3.2 from fresh electrolyte to 13.8 after 250 privacy cycles. We then explored the use of an inert core mesh (SS) where RME capacity was pre-loaded via electrodeposition of Cu and Bi. The use of a thin electroplated Au layer improves metal adhesion and RME of Cu and Bi compared to bare SS by reducing the onset potential for metal deposition by 128 mV and the onset potential

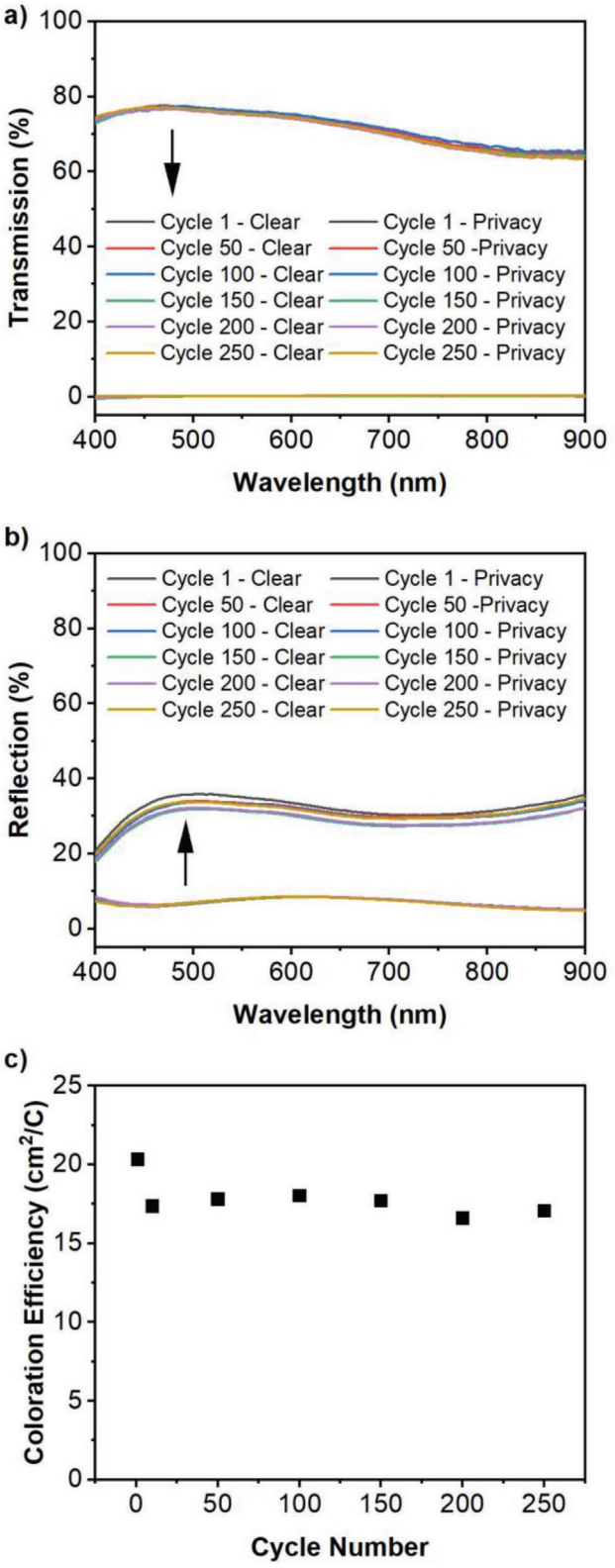

Figure 6. Cu—Bi Au-SS mesh RME dynamic window device performance over 250 privacy cycles: a) transmission versus wavelength, b) reflection versus wavelength, and c) coloration efficiency as a function of cycle number. Arrows in (a) and (b) indicate direction of window tinting. Windows were tinted at –0.7 V and bleached at +0.7 V.

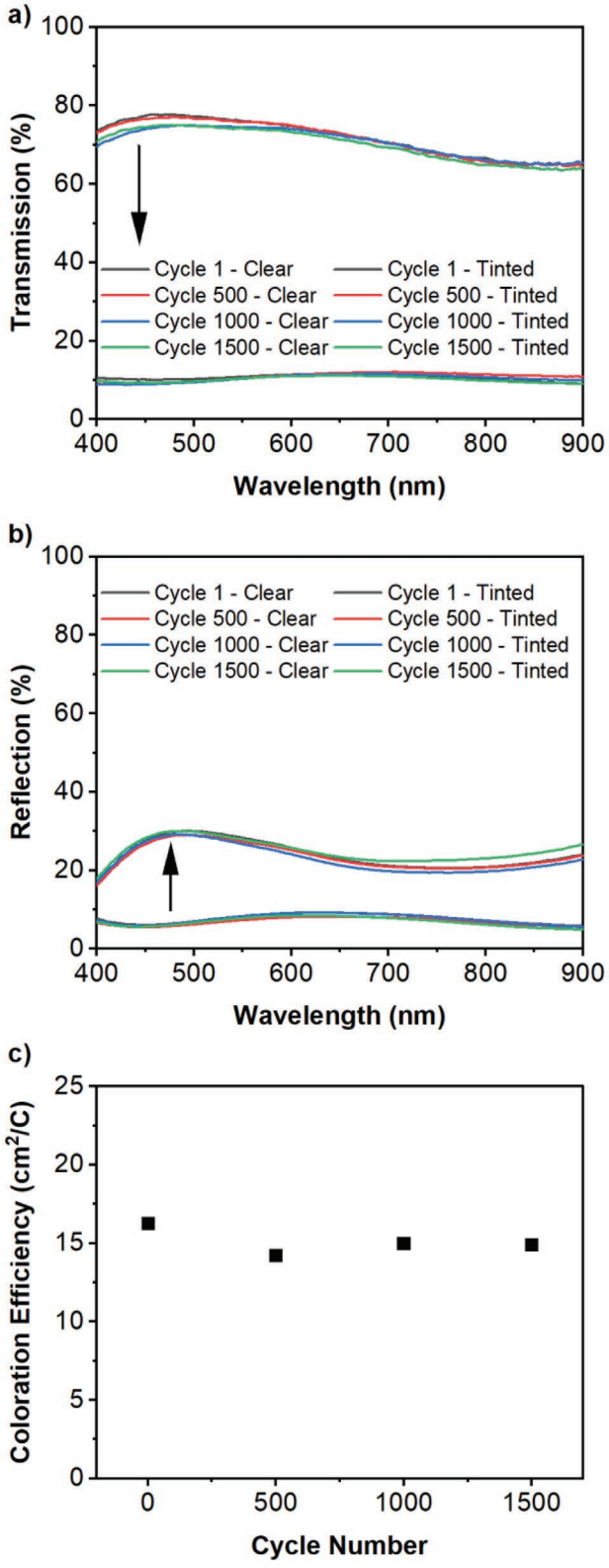

Figure 7. Cu—Bi Au-SS mesh RME dynamic window device performance over 1500 cycles to 10% dark state: a) transmission versus wavelength, b) reflection versus wavelength, and c) coloration efficiency as a function of cycle number. Arrows in (a) and (b) indicate direction of window tinting. Windows were tinted at –0.7 V and bleached at +0.7 V.

for metal stripping by 84 mV. With this improvement, we preload the Au-SS metal mesh with Cu—Bi (1.5 C cm^{-2}) with minimal transmission loss (80.5% to 78.8%) and low haze (0.8%). We then use this custom metal mesh design as a counter electrode material to make an RME window with consistent optical properties and coloration efficiency over 250 privacy cycles, and we give context this reported cycle number by cycling a device using this architecture to 10% dark state transmission, extending the cycle life to 1500 cycles. Finally, we implement this mesh in a 10 cm × 10 cm device to show uniform tinting at a large scale. This counter electrode design is the first demonstration of durable privacy cycling and paves the way towards making RME dynamic windows ubiquitous.

4. Experimental Section

Metal Counter Electrode Preparation: Cu mesh (100 mesh Copper 0.0012″ Wire Dia) and SS mesh (50 Mesh T316 Stainless High Transparency 0.0012″ Wire Dia) were bought from TWP, Inc. Cu foil was purchased from a local hardware store. The metal electrodes were sonicated in acetone then DI water for 10 min each, then dried in an oven at 120 °C. The Cu electrodes were then ready for use. The SS mesh was electrocleaned at 48 z at –7 V for 5 min using a SS rod as both a counter and reference electrode (Electro-Cleaner Solution, Gold Plating Services). The SS mesh was then rinsed with DI water before being submerged in the TriVal 24 K Acid Gold strike bath at room temperature at –7 V for 1 second using a Pt plated Ti rod as both a counter and reference electrode (TriVal Gold Strike, Gold Plating Services). The SS mesh was again rinsed with DI water then Cu and Bi were electroplated at –0.7 V versus Ag/AgCl using the Cu—Bi electrolyte and a Pt wire counter electrode to the desired capacity. The Cu—Bi Au-SS mesh was then rinsed in DI water then dried at 120 °C for 2 h before use.

Electrolyte Preparation: Chemicals were bought and used without purification. The electrolyte used for all metal plating experiments consisted of 10 mM $Cu(ClO_4)_2 \cdot 6H_2O$ (ACROS Organics), 10 mM $BiOClO_4 \cdot H_2O$ (GFS Chemicals), 10 mM $HClO_4$ (Alfa Aesar), 1 M $LiClO_4 \cdot 3H_2O$ (ACROS Organics) with 0.1 w/v% PVA (31000–50000 g/mol, 97% hydrolyzed, Aldrich) additive. PVA was added last and stirred at 1200 rpm and 60–70 °C until dissolved. "Blank" electrolytes did not have any active metals ($Cu(ClO_4)_2$ or $BiOClO_4$).

Pt-Modified TCO Working Electrode Preparation: ITO and fluorine tin oxide (FTO) on glass substrates (Xinyan Technology Ltd, nominal sheet resistance of 10 Ω $\square^{-1}$) were used as the TCO for RME dynamic windows. The TCO substrates were cleaned by sonication in 10% Extran in DI water solution, pure DI water, acetone, then isopropyl alcohol for 15 min each. After, the substrates were dried with N_2 then cleaned in a UV-Ozone cleaner for 15 min. The TCO substrates were then placed in a 10 mM 3-mercaptopropionic acid in ethanol solution and placed on a shaker for 24 h. The TCO substrates were then rinsed with ethanol then water before being placed in a Pt-nanoparticle solution (Sigma Aldrich) diluted 1:19 with DI water and placed on a shaker for 24–72 h. The TCO substrates were then rinsed with DI water, dried with N_2, then annealed at 250 °C for 25 min before use.

RME Dynamic Window Fabrication: Two-electrode devices used Pt-modified TCO on glass substrates (Pt-TCO) as a working electrode and a metal counter electrode. The 10 cm × 10 cm device shown in Figure 8 used Pt-FTO as the working electrode. All other devices used Pt-ITO as the working electrode. Two to three layers of butyl rubber edge seal (Quanex: Solargain edge tape LP03, 1.5 mm thickness) separated the two electrodes and encapsulated the electrolyte between the Pt-TCO and back piece of glass. Conductive tape (Conducty Z22, ElectricMosaic) was used to make electrical contact with the working electrode. See Figure S26, Supporting Information, for design schematic.

Electrochemical Characterization and Device Cycling: Electrochemical experiments were run using a BioLogic SP-50 or SP-150 potentiostat.

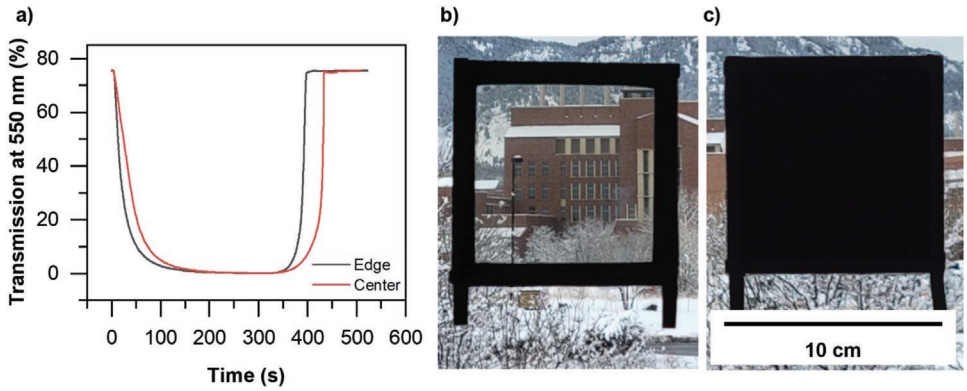

Figure 8. a) Transmission at 550 nm versus time at the edge (black) and center (red) of 10 cm × 10 cm device using the Cu—Bi Au-SS mesh. b,c) Images of the 10 cm × 10 cm device in the b) clear and c) privacy states. Windows were tinted at –0.7 V for tinting and bleached at +0.7 V.

Three-electrode experiments used a Pt wire counter electrode and a "no-leak" Ag/AgCl (eDAQ) reference electrode. Two-electrode devices were cycled at –0.7 V until the charge required for cycling was passed for window tinting: 159 mC cm^{-2} for the Cu mesh device and 147 mC cm^{-2} for the Cu—Bi Au-SS mesh device for privacy cycling, 61 mC cm^{-2} for 10% dark state transmission cycling, and +0.7 V until transparency was restored for window bleaching. Check in cycles were run by ensuring desired transmission states were reached.

Optical Characterization: Ocean Optics OCEAN FX Miniature spectrometer was used in a standard configuration with an Ocean Optics halogen light source (HL-2000) for most transmission and all reflection measurements.

Remaining transmission measurements (total and diffuse transmission) were conducted using a Varian CARY 500 UV–Vis–NIR Spectrophotometer equipped with a 150 mm integrating sphere. The experimental setup for the haze coefficient characterization based on these integrating sphere and spectrophotometer followed the ASTM D1003 standard, which is the accepted standard for haze measurements for window applications.

Characterization: SEM-EDS was run using a HITACHI SU3500 scanning electron microscope operated at an accelerating voltage of 15 kV and equipped with an EDS detector.

Supporting Information

Supporting Information is available from the Wiley Online Library or from the author.

Acknowledgements

This research was funded by the National Science Foundation (NSF) under award number 2127308. A.L.Y. acknowledges the financial support of a Graduate Assistantship in Areas of National Need (GAANN) Fellowship from the U.S. Department of Education. E.A. and I.I.S. acknowledge the U.S. Department of Energy, Advanced Research Projects Agency-Energy grant DE-AR0000743 that supported the development of the optical characterization facility. The authors would like to thank Lori Postak from Quanex for providing the Solargain butyl rubber edge tape. The authors would also like to thank Robert Darger from Gold Plating Services for assistance with using their products and fruitful discussion. This research was supported in part by the Colorado Shared Instrumentation in Nanofabrication and Characterization (COSINC): the COSINC-CHR (Characterization) and/or CONSINC-FAB (Fabrication), College of Engineering & Applied Science, University of Colorado Boulder. The authors would like to acknowledge the support of the staff (Tomoko Borsa) and the facility that have made this work possible.

Conflict of Interest

T.S.H., M.T.S., and M.D.M. are co-founders of Tynt Technologies, a company commercializing dynamic windows.

Author Contributions

A.L.Y., T.S.H., M.T.S., and M.D.M. designed the experiments. A.L.Y., T.S.H., M.T.S., C.J.B., I.I.S., and M.D.M. analyzed the data. A.L.Y., T.S.H., M.T.S., E.A., and D.J.S. performed the experiments. A.L.Y. and M.D.M. wrote the paper. All authors discussed the results and commented on the manuscript.

Data Availability Statement

Research data are not shared.

Keywords

dynamic windows, electrochemistry, reversible metal electrodeposition, transparent metal mesh

Received: March 11, 2022
Revised: May 25, 2022
Published online:

[1] View, *Energy Benefits of View Dynamic Windows*, **2015**, https://view.com/assets/pdfs/workplace-white-paper.pdf.
[2] C. Craig, M. Gregorio, *Natural Light Is the Best Medicine for the Office*, **2018**, https://view.com/sites/default/files/documents/daylight-research.pdf.
[3] M. Krarti, *J. Build. Eng.* **2022**, *45*, 103462.
[4] A. Hedge, D. Nou, *Ergon. Int. J.* **2018**, *2*, 1.
[5] C. G. Granqvist, M. A. Arvizu, İ. Bayrak Pehlivan, H.-Y. Qu, R.-T. Wen, G. A. Niklasson, *Electrochim. Acta* **2018**, *259*, 1170.
[6] J. S. E. M. Svensson, C. G. Granqvist, *Sol. Energy Mater.* **1984**, *11*, 29.
[7] R. J. Mortimer, A. L. Dyer, J. R. Reynolds, *Displays* **2006**, *27*, 2.

[8] V. K. Thakur, G. Ding, J. Ma, P. S. Lee, X. Lu, *Adv. Mater.* **2012**, *24*, 4071.
[9] D. R. Rosseinsky, R. J. Mortimer, *Adv. Mater.* **2001**, *13*, 783.
[10] View, *View Dynamic Glass Product Guide*, **2019**, https://view.com/product.
[11] SageGlass, *SageGlass Product Guide*, **2016**, https://www.sageglass.com/en/products/sageglass.
[12] Halio, *Halio Black Insulated Glass Unite (IGU)*, **2021**, https://halioinc.com/resource-categories/glazing-datasheets/.
[13] G. Burrell, *Visible Light Transmission and Visual Comfort*, **2020**, https://view.com/sites/default/files/documents/view-light-transmission-visual-comfort-white-paper.pdf.
[14] M. T. Strand, T. S. Hernandez, M. G. Danner, A. L. Yeang, N. Jarvey, C. J. Barile, M. D. McGehee, *Nat. Energy* **2021**, *6*, 546.
[15] X. Tao, D. Liu, J. Yu, H. Cheng, *Adv. Opt. Mater.* **2021**, *9*, 2001847.
[16] C. J. Barile, D. J. Slotcavage, J. Hou, M. T. Strand, T. S. Hernandez, M. D. McGehee, *Joule* **2017**, *1*, 133.
[17] T. S. Hernandez, C. J. Barile, M. T. Strand, T. E. Dayrit, D. J. Slotcavage, M. D. McGehee, *ACS Energy Lett.* **2018**, *3*, 104.
[18] M. T. Strand, C. J. Barile, T. S. Hernandez, T. E. Dayrit, L. Bertoluzzi, D. J. Slotcavage, M. D. McGehee, *ACS Energy Lett.* **2018**, *3*, 2823.
[19] T. S. Hernandez, M. Alshurafa, M. T. Strand, A. L. Yeang, M. G. Danner, C. J. Barile, M. D. McGehee, *Joule* **2020**, *4*, 1501.
[20] S. Araki, K. Nakamura, K. Kobayashi, A. Tsuboi, N. Kobayashi, *Adv. Mater.* **2012**, *24*, OP122.
[21] M. Son, D. Shin, C. S. Lee, *Adv. Mater. Interfaces* **2021**, *8*, 2001416.
[22] S. M. Islam, T. S. Hernandez, M. D. McGehee, C. J. Barile, *Nat. Energy* **2019**, *4*, 223
[23] S. M. Islam, A. A. Palma, R. P. Gautam, C. J. Barile, *ACS Appl. Mater. Interfaces* **2020**, *12*, 44874.
[24] S. M. Islam, C. J. Barile, *ACS Appl. Mater. Interfaces* **2019**, *11*, 40043.
[25] S. Kimura, K. Nakamura, N. Kobayashi, *Sol. Energy Mater. Sol. Cells* **2020**, *205*, 110247.
[26] A. C. Sonavane, A. I. Inamdar, P. S. Shinde, H. P. Deshmukh, R. S. Patil, P. S. Patil, *J. Alloys Compd.* **2010**, *489*, 667.
[27] B. Wen-Cheun Au, K. Y. Chan, D. Knipp, *Opt. Mater.* **2019**, *94*, 387.
[28] D. S. Dalavi, M. J. Suryavanshi, D. S. Patil, S. S. Mali, A. V. Moholkar, S. S. Kalagi, S. A. Vanalkar, S. R. Kang, J. H. Kim, P. S. Patil, *Appl. Surf. Sci.* **2011**, *257*, 2647.
[29] D. M. DeLongchamp, P. T. Hammond, *Chem. Mater.* **2004**, *16*, 4799.
[30] D. S. Ghosh, T. L. Chen, V. Pruneri, *Appl. Phys. Lett.* **2010**, *96*, 041109.
[31] M. Luo, Y. Liu, W. Huang, W. Qiao, Y. Zhou, Y. Ye, L.-S. Chen, *Micromachines* **2017**, *8*, 12.
[32] J. H. Cho, D. J. Kang, N.-S. Jang, K.-H. Kim, P. Won, S. H. Ko, H. Ko, J.-M. Kim, *ACS Appl. Mater. Interfaces* **2017**, *9*, 40905.
[33] H. Li, W. Zhang, A. Y. Elezzabi, *Adv. Mater.* **2020**, *32*, 2003574.
[34] H. B. Lee, W. Y. Jin, M. M. Ovhal, N. Kumar, J. W. Kang, *J. Mater. Chem. C* **2019**, *7*, 1087.
[35] M. Dressel, G. Gruener, G. F. Bertsch, *Am. J. Phys.* **2002**, *70*, 1269.
[36] A. Khan, S. Lee, T. Jang, Z. Xiong, C. Zhang, J. Tang, L. J. Guo, W.-D. Li, *Small* **2016**, *12*, 3021.
[37] T. Gao, Z. Li, P. S. Huang, G. J. Shenoy, D. Parobek, S. Tan, J. K. Lee, H. Liu, P. W. Leu, *ACS Nano* **2015**, *9*, 5440.
[38] S. De, J. N. Coleman, *ACS Nano* **2010**, *4*, 2713.
[39] T. Sannicolo, M. Lagrange, A. Cabos, C. Celle, J. P. Simonato, D. Bellet, *Small* **2016**, *12*, 6052.
[40] Y. Jang, J. Kim, D. Byun, *J. Phys. D: Appl. Phys.* **2013**, *46*, 155103.
[41] S. Hassab, D. E. Shen, A. M. Österholm, M. Da Rocha, G. Song, Y. Alesanco, A. Viñuales, A. Rougier, J. R. Reynolds, J. Padilla, *Sol. Energy Mater. Sol. Cells* **2018**, *185*, 54.
[42] X. Zhu, M. Liu, X. Qi, H. Li, Y. F. Zhang, Z. Li, Z. Peng, J. Yang, L. Qian, Q. Xu, N. Gou, J. He, D. Li, H. Lan, *Adv. Mater.* **2021**, *33*, 2007772.
[43] J. Jang, H. G. Im, J. Jin, J. Lee, J. Y. Lee, B. S. Bae, *ACS Appl. Mater. Interfaces* **2016**, *8*, 27035.
[44] S. T. Singleton, J. J. O'Dea, J. Osteryoung, *Anal. Chem.* **1989**, *61*, 1211.
[45] H. Le, R. G. Compton, *J. Electroanal. Chem.* **2020**, *866*, 114149.
[46] A. J. Bard, L. R. Faulkner, *Electrochemical Methods: Fundamentals and Applications*, Wiley, New York **2001**.
[47] S. Zaromb, *J. Electrochem. Soc.* **1962**, *109*, 903.
[48] S. M. Islam, C. J. Barile, *Adv. Energy Mater.* **2021**, *11*, 2100417.
[49] ASTM, *Standard Practice for Preparation of and Electroplating on Stainless Steel 1*, **1998**, https://www.astm.org/b0254-92r20e01.html.
[50] C. J. Barile, *J. Appl. Electrochem.* **2018**, *48*, 443.
[51] T. Guena, P. Leblanc, in *INTELEC 06 - Twenty-Eighth International Telecommunications Energy Conference*, IEEE, New York **2006**.
[52] S. Watanabe, M. Kinoshita, T. Hosokawa, K. Morigaki, K. Nakura, *J. Power Sources* **2014**, *258*, 210.